IEEE Access
Multidisciplinary | Rapid Review | Open Access Journal

Received 11 September 2023, accepted 24 September 2023, date of publication 27 September 2023,
date of current version 3 October 2023.

Digital Object Identifier 10.1109/ACCESS.2023.3320048

RESEARCH ARTICLE

Detection of Biotic or Abiotic Stress in Vineyards Using Thermal and RGB Images Captured via IoT Sensors

GEORGIOS FEVGAS[1], THOMAS LAGKAS[1], (Senior Member, IEEE), VASILEIOS ARGYRIOU[2], (Member, IEEE), AND PANAGIOTIS SARIGIANNIDIS[3], (Member, IEEE)

[1]Department of Computer Science, International Hellenic University, 65404 Kavala, Greece
[2]Department of Networks and Digital Media, Kingston University, KT1 2EE Surrey, U.K.
[3]Department of Electrical and Computer Engineering, University of Western Macedonia, 50100 Kozani, Greece

Corresponding author: Georgios Fevgas (gefevga@cs.ihu.gr)

The publication of the article in OA mode was financially supported by HEAL-Link.

ABSTRACT The abiotic and biotic plant stress is a critical factor for the agriculture industry, considering that plant stress increases production costs and reduces the quantity and quality of the output product. The early detection of plant stress using new technologies and even more utilizing Internet of Things (IoT) sensors is significant for the growers to act as early as a problem is in the nascent. Furthermore, the insights from the early detection of plant stress can be used as actionable data for fertilization and pesticide optimization. Our proposed state-of-the-art method uses Thermal Infrared (TIR) and high-resolution visible-spectrum (RGB) images acquired by IoT sensors of Unmanned Aerial Vehicles (UAVs) from two experiment vineyards (Vitis vinifera L.) for two years in a total of twelve flights. The OTSU method is used for the plants' canopy isolation from the soil. The k-Means clustering is used in the relative temperature values of the plant's canopy to detect the leaves' stomatal closure. The clusters' pixel coordinates of the TIR image, which represents leaves' stressed areas, are used, and a pseudo-coloring of yellow is assigned in the corresponding pixels of the aligned RGB image. Finally, an RGB image is generated with yellow pseudo-coloring over the stressed areas of the vineyards' canopy. The stressed plants caused by abiotic and biotic factors were validated and compared with the Triangular Greenness Index (TGI), which measures the leaf chlorophyll content like other multispectral indexes. Finally, the proposed method shows significantly higher accuracy and precision than TGI based on the two years of experimentation results, considering that the F1-score of the proposed method is better than TGI in the cumulative of the two years by 70.55%.

INDEX TERMS Internet of Things (IoT), thermal infrared (TIR), crop stress, precision viticulture, remote sensing, temperature, transpiration.

I. INTRODUCTION

Due to the rapid technological development in recent years, various sensors and the Internet of Things (IoT) have been developed that can be used to collect data on crops. These are visual cameras (RGB), spectral sensors, Light Detection and Ranging (LiDAR), and thermal infrared cameras. Some of their applications are plant height control, biomass, Leaf Area Index (LAI), and other essential physiological characteristics, considering that plant diseases are the most common cause of production and economic loss [1], [2]. Even more, pathogens are the leading cause of yield losses of 20-40% globally [3].

Furthermore, IoT sensors have more accuracy and higher resolution when referring to imaging spectrums than satellites with low image resolution. However, Very Low Earth Orbit (VLEO) satellites carrying high-resolution sensors are under development.

The associate editor coordinating the review of this manuscript and approving it for publication was Alessandro Pozzebon.

The use of visual cameras (RGB) is more common than other sensors because they have low cost, are lightweight, and have simple data processing. Their disadvantages are low radiometric resolution and lack of proper calibration [4], [5]. They can be used in the rapid acquisition of color photographs to calculate the height of the crop, the LAI, and the color of the leaves so that through already developed algorithms with the image processing method, the damaged ''dry'' leaves can be detected. However, this method lags in obtaining phenotype information and crop characteristics due to the need for a visible camera to capture the invisible spectrum [6], [7]. Hunt et al. [8] propose the Triangular Greenness Index (TGI) method based on the visible spectrum, which is affected only by leaf chlorophyll content. The TGI can detect the leaf nitrogen content and other problems such as plant disease or insect damage because of leaves' chlorophyll content reduction.

Multispectral sensors can receive radiation in the visible and non-visible spectrum, which can be used to obtain a crop's phenotype [9]. Their main disadvantages are complex data processing and sensitivity to weather conditions [10], [11], [12], [13].

The determination of ranges by the LiDAR sensor is accomplished through laser-based targeting of an object, utilizing the photoelectric detection technique. It can be used to measure biomass and plant height. Its advantage is the effective acquisition of high-precision horizontal and vertical vegetation structures. Its disadvantages are the high cost of acquisition and the large amounts of data processing [14], [15].

The comprehensive development of remote sensing for analyzing and controlling chlorophyll content, Leaf Area Index (LAI), and leaf nitrogen content has been achieved [4], [5]. Therefore, we can have accurate plant growth information because the leaves' spectral characteristics are directly related to the above indices.

The TIR camera uses infrared radiation. Therefore, it can be used to measure plants' canopy temperature, the rate of water vapor left from leaves, and the carbon dioxide (CO2) entering leaves [16]. By employing this method, it becomes feasible to assess the growth status of the crop indirectly.

Traditional methods using thermal infrared imaging have constraints due to the sensitivity of the plants' canopy temperature to environmental factors, such as the soil's effect, ambient temperature, and wind [17], [18], [19], [20].

Comprehensive methods combining TIR and RGB images with Machine Learning techniques are crucial for detecting plant stress and overcoming environmental factor constraints such as soil effects. The lack of research in this field impedes the progress toward a dependable method for a robust approach to efficient, precise, and early detection of plant stress.

We propose a new Machine Learning-based method that uses TIR and RGB images to cluster the canopy temperatures of plants, excluding soil interference. The result is a pseudo-color image with annotated plant areas with higher temperatures indicating stress. Our study aims to evaluate plant stress more accurately and efficiently using IoT sensors like TIR and RGB cameras. The objectives of this paper are the development of this innovative methodology, its experimental validation, and its contribution to enhancing agricultural technology. Ultimately, it will enable more accurate stress detection and informed decision-making, improving crop management practices based on actionable data.

This paper is organized as follows. Section II describes the definition of plant stress and the biotic and abiotic factors causing it. In Section III, we discuss related work, and in Section IV, we describe our experimental methodology. In Section V, we present the results of the proposed method. We conclude in Section VI, summarizing our main results and future work.

II. ABIOTIC AND BIOTIC STRESS IN PLANTS

The genetic potential of plants to achieve their maximum yield is often impeded by various factors such as inadequate water or nutrient supply, unfavorable climatic conditions, plant pathologies, and insect infestations, which ultimately hamper growth at some point. These biotic and abiotic constraints induce stress on the plants, elevating their canopy temperature compared to healthy ones. Physiological and anatomical changes occur in plants due to biotic-abiotic stress. If there is a scarcity of water or the presence of vascular diseases such as plant diseases and insect damage, the transpiration of leaf stomata will be constrained. Consequently, there will be a reduction in the cooling effect of the evaporating water on the leaf surfaces, causing a consequent increase in the temperatures of the leaves [21].

Historically, plant stress detection has relied on the visual inspection skills of experienced growers and agronomists who can discern subtle color changes or leaf drooping as stress indicators. However, these methods are limited by the subjective nature of visual interpretation and the difficulty of assessing large crops. Additionally, when visual or tactile signs of stress are evident, irreversible damage may have already occurred. Nonetheless, stress-induced changes in plant radiation can be detected through remote sensing techniques, specifically using a TIR camera, which quantifies plant stress resulting from biotic and abiotic factors [21].

The plants' infection with diseases and deficiencies changes the leaves' stomatal conductance. Also, the leaf temperature increase is a very early symptom of a stressed plant before the appearance of visible symptoms [22], [23]. Different environmental stresses such as salinity, nutrient deficiency, and biotic factors lead to a leaves' stomatal closure, which the thermal infrared spectrum band can detect [24]. Furthermore, TIR sensors are more effective than hyperspectral, multispectral, and visible sensors for the early detection of changes caused by diseases [23].

Due to the stomatal closure, the transpiration rates of the leaves decrease, and the leaves' surface temperature increases. A consequence of the stomatal closure is reducing the photosynthetic rate, which decreases the chlorophyll

content, which can be detected using the multispectral band [25]. Finally, the last stage of a stressed plant is reducing the leaves' surface due to foliage's necrosis.

As described above in the definition of plant stress, the factors that cause it can be biotic, abiotic, or a combination. Therefore, below is a detailed description of each factor that can be detected in the longwave infrared (LWIR) range of 8 - 14 μm (Thermal Infrared - TIR) and how it affects the radiant temperature of the leaf. Also, below is a reference to research that proves plant leaves' temperature increases if biotic and abiotic factors are present.

A. ABIOTIC FACTORS

Abiotic stress factors impacting plant health include high temperatures, low temperatures, excess moisture, water scarcity, nutrient imbalances, and saline conditions.

1) WATER STRESS

The methodology applied on the whole crop and not on each plant is the Crop Water Stress Index (CWSI), which determines a crop's water availability using infrared temperature measurements of the plant's canopy. The plant's crown's temperature indicates the culture's aqueous condition because the foliage's stomata close in response to the water's depletion, causing a decrease in transpiration and increasing the temperature of the leaf. On the contrary, the adequacy of water in the soil keeps the stomata open and a strong respiration rate, resulting in a decrease in the foliage's temperature compared to the atmospheric temperature above the crop [26]. Studies have demonstrated that plants experiencing biotic or abiotic stress display elevated canopy temperatures compared to their healthy counterparts [27], [28].

Following four days of flooding, the cotton crop's crown experienced a minor increase in air temperature, despite submerging 60% of its root system. However, signs of stress were observed on the eighth day when the flooded plants exhibited dome temperatures of 4-6 degrees Celsius higher than those of plants with roots in drained soil [21].

2) TEMPERATURE STRESS

Plants can be negatively impacted by temperatures falling outside their preferred growth range. Heat stress can occur when plants are exposed to higher temperatures than usual, causing protein denaturation and reduced photosynthesis due to dehydration. Cold stress can also occur when temperatures drop below the optimal range for growth, leading to the development of ice crystals within cells, which can cause cellular damage.

Fuller and Wisniewski [29] conducted a study using a thermal camera to record ice nucleation in potatoes and cauliflower. The thermal imaging revealed that the average temperature of the leaves of both species increased during freezing.

Stenger et al. [30] utilized infrared thermography to study the relationship between ice formation and frost injury in potato leaves. The results indicate an increase in leaf temperature, as ice nucleation is an exothermic process.

Costa et al. [31] presented a study using a thermal camera to measure vineyards' canopy and soil temperature for better water and heat stress management. The findings revealed that the canopy temperature can indicate grapevine performance, and the soil temperature can be used as a potential variable for managing heat and drought stress in the vineyard.

3) NUTRIENT STRESS

The nutrients are necessary for the growth and development of the plants. When the plants lack nutrients such as Nitrogen, Calcium, or Iron, they can exhibit various symptoms, such as an increase in the leaf's temperature, which indicates nutrient stress.

Pan et al. [32] presented a study that compared the growth and photosynthetic characteristics of cotton varieties under hypoxia stress. The TIR imaging showed that the plants under hypoxia stress had low stomatal conductance and increased leaves' temperature.

Chaerle et al. [33] used visible, fluorescence, and thermal imaging to detect early nutrient magnesium deficiency in bean plants. The results show that the thermal infrared camera found a necrotic lesion due to magnesium deficiency at the 7-day time point.

4) SALINITY STRESS

In arid regions, the augmented salinity of soil can be attributed to the frequent irrigation of crops. Timely identification of salt-affected regions can facilitate the implementation of preventive measures prior to extensive harm being incurred upon the crop [21].

According to Myers et al. [34], an elevation in salinity equivalent to 16 dS mI (= mMho / cm) resulted in a rise of approximately 11 °C in the temperature differential between the crop dome and the ambient air. Additionally, under elevated salinity and vapor deficits typical of irrigated regions, vegetation exhibited stress symptoms, despite an absence of constraints on soil moisture.

Siddiqui et al. [35] measured the response of rice in different treatments of salt stress environments using a TIR camera with constant temperature and humidity. The results show that the plant's temperature also increased as the salinity increased.

Sirault et al. [36] presented a study of automated image analysis using a TIR camera to quantify the osmotic stress response of barley and wheat to salinity. The results show that as the osmotic stress increases due to salt treatment, the leaf's latent heat flux and transpiration decrease, consequently increasing the plant's canopy temperature.

B. BIOTIC FACTORS

The main entry point for pathogens into plants is through the stomata of leaves, leading to the usual defense response of stomatal closure. Additionally, herbivore insects can cause

direct damage to leaves and stems, resulting in stomatal closure. Thus, biotic stress factors like insects and pathogens (viruses, bacteria, fungi, oomycetes, and nematodes) significantly impact plant health.

1) DISEASES' STRESS

The disruption of its vascular permeability can increase the resistance and temperature of a plant's dome due to diseases or insects. Pinter et al. [37] employed a thermal-infrared radiometer to determine the temperatures of sugar beet leaves contaminated with Pythium aphanidermatum. Their findings revealed that the leaf temperatures of diseased plants were approximately 2.6-3.6 °C higher than those of healthy plants, even though the disease was not visibly noticeable without root examination. Furthermore, diseased plants maintained higher leaf temperatures under Water Stress conditions than healthy plants.

Similar results were obtained for infected cotton by Pymatotrichum omnivorum, where plants with moderate disease intensity had sunlit leaves that were 3.3-5.3 °C warmer than those without any fungal infection. One day after watering, the temperature difference between diseased and healthy plants was noticeable, and as soil moisture decreased, diseased plants withered first [21].

In a greenhouse study, Nilsson [38] found that rapeseed leaves infected with Verticillium dahliae had leaf temperatures that were 5-8 °C higher than uninfected plants due to the disease's induction of stomatal closure.

Wang et al. [39] used chlorophyll fluorescence (ChlF) and TIR non-destructive imaging in sweet potatoes to detect virus diseases that caused the Sweetpotato feathery mottle virus (SPFMV) and Sweetpotato chlorotic stunt virus (SPCSV) co-infection. After 29 days of monitoring of viral infection in Sweetpotato, the results show that the TIR imaging can be used as an indicator for the severity of viral infection after the first week of growth.

2) INSECT STRESS

Insects cause plant stress by interrupting stomatal transpiration due to damage to the leaves and stems. As the leaves' structure is destroyed and the stomata close, the temperature of the leaves increases [21].

Joalland et al. [40] presented a study using visible light imaging, thermography, and spectrometry to evaluate the effect of the disease pressure of Beet Cyst Nematodes (BCN) on sugar beets. The results of the thermography used to evaluate the plants' canopy temperature show that the canopy temperature of the plants infected with nematode was higher than that of healthy plants.

Ortiz-Bustos et al. [41] used blue-green fluorescence (BGF) and thermal imaging to detect the root parasitic weed of Orobanche cumana Wallr on sunflowers. The thermal imaging results show that the parasite-infected sunflowers had warmer leaves due to stomatal closure and transpiration reduction.

As described above, the plant will be stressed if there is a biotic or abiotic factor. When a plant is stressed, some leaves or the whole canopy will increase the temperature, depending on the stress factor. For example, if an insect contaminates a leaf initially, it will cause stress on that leaf and, consequently, a temperature increase.

III. RELATED WORK

In the literature, there has been much work on using thermal infrared and visible imaging to monitor the crop's growth and detect the water stress of the plants [18], [42]. Thermal imaging can be used for the crop's stress monitoring considering the relation between the canopy temperature, stomatal conductance, and leaf transpiration rate [16].

In later years is known that a conventional method of using a handheld TIR camera has the limitation of capturing images of the whole crop in a small-time amount. On the other hand, using UAVs equipped with a TIR camera can quickly capture the crop canopy temperature, identifying the temperature differences between the plants.

Berni et al. [43] proposed a model based on olive trees' canopy temperature from airborne thermal infrared imaging to calculate tree canopy conductance (Gc) and the CWSI. They validated that Gc and CWSI are directly related to the stomata transpiration of the olive trees, which are affected by water deficiency.

Gonzalez-Dugo et al. [18] presented a study using the thermal index CWSI on experimental wheat fields, which validates that thermal infrared imaging can be used for crop growth monitoring and water stress.

Berni et al. [44] presented a study using high-resolution thermal infrared images acquired from a UAV of a peach orchard field. They found a thermal variation in the plants due to variations in irrigation levels of the field, which validate the water stress detection in plants using airborne thermal infrared imaging.

Jones et al. [19] measured the leaf temperature of vineyards using a TIR camera carried by a UAV. They used three irrigation treatments in three vineyard areas and validated the mean canopy temperature and the plants' stomatal conductance response according to water deficiency.

Falkenberg et al. [45] presented a remote sensing method of biotic and abiotic stress using a TIR camera in cotton fields. The results show that the thermal infrared camera detected biotic stress before visible symptoms on cotton and can discriminate the abiotic from biotic stress.

Cohen et al. [46] presented a study using thermal infrared imaging for the early detection of Downy Mildew (Peronospora) in Grapevine (Vitis vinifera L.). They collected TIR images of infected and healthy plants at different day hours. The results show that downy mildew can be detected before visible symptoms using thermal infrared imaging.

Smigaj et al. [47] investigated the potential use of UAVs with a TIR camera to detect Dothistroma septosporum disease on pines. The authors found a significant correlation

between canopy temperature and disease levels, especially during morning flights with peak photosynthetic activity.

Wang et al. [48] used thermography in wheat infected by the fungus Zymoseptoria triciti to predict the disease before symptoms expressed on the plants. The results show a significant correlation between the canopy temperature and the disease level, which means the ability to predict the early stages of the fungal infection in wheat.

Park and Kim [49] conducted a study using infrared thermography to compare the temperatures of healthy leaves and those with necrotic spots on oriental cherry, Japanese cornel, and sawtooth oak. The results indicate a significant difference in temperature between healthy and diseased leaves.

López-López et al. [50] presented a study using thermal and hyperspectral airborne imagery for the early detection of red leaf blotch in almond orchards. The authors used classification methods such as linear discriminant analysis and support vector machine in a combination of vegetation indices to classify the disease severity of the red leaf blotch. The results show that the proposed method can detect and quantify the red leaf blotch.

Zhang et al. [51] presented a study using thermal and high-resolution RGB images captured by a UAV to extract the canopy temperature of maize. The authors proposed a method of red-green ratio index (RGRI)-Otsu for the extraction of the canopy temperature. The results show a high correlation between the maize's canopy temperature and the ground-truth temperatures captured by a handheld infrared thermometer.

The Triangular Greenness Index (TGI) is based on chlorophyll spectral features, and it can measure the leaf chlorophyll content related to low leaf nitrogen content, plant diseases, or other deficiencies [8]. The TGI was selected as a comparison index of our proposed method because of the constraint of the hardware (TIR and visual camera) used for image acquisition. Compared with other indexes, one more advantage of the TGI method is that it needs only a visible camera because the bands used in the TGI's equation are in the visible spectrum. Furthermore, TGI is calculated by three points of the visible wavelength, which are 480 nm, 550 nm, and 670 nm. The equation of TGI is: $\mathrm{TGI} = -0.5[190(\mathrm{R670}–\mathrm{R550}) - 120(\mathrm{R670}–\mathrm{R480})]$, where R is the reflectance at wavelength.

In the results section, except for our proposed method's output images with stressed plants, TGI is used as a comparison index measuring the chlorophyll content like other multispectral indexes.

IV. METHODOLOGY

Our work is focused on thermal infrared and RGB images captured from remote sensing using Unmanned Aerial Vehicles. The proposed solution aims to eliminate the soil's pixels from the TIR image and find the leaves' pixels under stress considering the relative pixels' temperatures of the plant's canopy. However, our empirical results validate the relationship between leaves' high temperatures and stomatal closure, resulting from an abiotic, biotic stress factor.

A. FIELD SELECTION

Two grapevines (Vitis vinifera L.) were selected for the experiments in Askri, Viotia, Greece, of the Muses Estate. Both grapevines, Vitis vinifera (L.) cv. Mouhtaro vineyard (38.325104 N, 23.093501 E, Altitude: 480 m), and Vitis vinifera (L.) cv. Merlot vineyard (38.325817 N, 23.092826 E, Altitude: 480 m) were eleven years old on the date of the first coverage. The images were captured starting from 2021 until 2022. Every year, each vineyard is surveyed three times in the stages of flowering, fruit set, and veraison of the grapevine lifecycle. Each vineyard was surveyed six times in two years. Both vineyards received the same fertilization, pest, and disease management treatment.

B. IMAGES ACQUISITION

Two types of multi-rotor UAVs were used for field surveying during the two years. In the first year, the DJI Matrice 200 (SZ DJI Technology Co., Ltd., China) was used with the dual camera FLIR Duo Pro R 640 (Teledyne FLIR LLC., USA). The DJI Mavic 2 Enterprise Advanced (SZ DJI Technology Co., Ltd., China) was used in the second year.

The drones' cameras mentioned above can capture two (2) images simultaneously, an RGB image with an embedded thermal infrared image and one TIR and one RGB image with metadata, respectively. The TIR cameras' spectrum (Thermal Infrared Spectral Band) is 8 - 14 μm. In two years of surveys and twelve flights, a total of 4660 images were captured, where 2330 are RGB images and the other 2330 are TIR images.

A boustrophedon Coverage Path Planning (CPP) method was used for surveying vineyards by every multi-rotor UAV to capture the same vines with the same sequence in every flight. The flying altitude is computed according to Ground Sample Distance (GSD), considering the UAVs' thermal infrared sensors' resolution. The GSD pertains to the measurement between centers of pixels on the ground, and a smaller GSD value corresponds to a more excellent spatial resolution of the image. The entire dataset of TIR images obtained for two years was preserved at an approximate GSD of 3 cm, translating to a resolution of 3 cm per pixel.

C. DATA SPECIFIC PARAMETERS

The multi-rotor UAVs surveyed the fields according to the GSD of the TIR camera; the flight altitude was approximately 20 meters, and the front and side overlapped, which used 75%. The specific parameters of the TIR and RGB images of both cameras, such as focal length, resolution, bit depth, megapixels, field of view, and compression, are presented in Table 3.

D. IMAGES PRE-PROCESSING

Prior to utilizing the TIR and RGB images alongside their accompanying metadata, it is imperative to undergo pre-processing procedures that involve alignment and soil elimination.

1) IMAGES ALIGNMENT

For the alignment of the TIR and RGB images, some metadata variables were used, specifically:

- The Real2Ir variable is the factor by which we need to multiply the TIR image to be the same size as the RGB image.
- The offsetX and offsetY variables are the offset pixels between TIR and RGB images on the X and Y axis.
- The width and the height of the RGB and TIR images.

Initially, to determine the resize percentage of the RGB image according to the TIR image size, the variable of Real2Ir, the Width of the RGB image, and the Width of the TIR image are used as shown in (1).

$$Resize\_percentage = 100 \times \frac{RGBImageWidth}{\frac{Real2Ir}{ThermalImageWidth}} \quad (1)$$

The next step before the crop of the RGB image is to offset according to the values of the metadata variables OffsetX and OffsetY, which presents the pixels' offset between the RGB and TIR images.

After offsetting, the RGB image is cropped based on Resize_Percentage and TIR Image Width and Height. The cropped values for X-axis and Y-axis are computed as shown in (2) and (3).

$$CropX = Resize\_Percentage \times \frac{Thermal\_Image\_Width}{100} \quad (2)$$

$$CropY = Resize\_Percentage \times \frac{Thermal\_Image\_Height}{100} \quad (3)$$

Finally, the pixels of the cropped RGB image are equivalent (spatially - exact coordinates) to each pixel of the TIR image.

2) SOIL ISOLATION

Considering that the pixels of the thermal infrared images used in our method are only vegetation, specifically the canopy leaves of the vineyards, a surface emissivity of 0.98 was set and used in TIR images [52], [53].

One of the most known problems is eliminating the soil in the TIR image. Giuliani and Flore [54], proposed a method using a sheet background that heats up above the plant's temperature and can exclude it from the image considering the TIR image's histogram.

Another approach for soil elimination is identifying leaves' pixels from an RGB image and extracting only the temperatures from the corresponding pixels of the TIR image [55], [56].

Gonzalez-Dugo et al. [42] used the OTSU method to extract the canopy temperature automatically. However, a constraint of the OTSU method is that the threshold pixels usually contain soil pixels. Furthermore, it is difficult to extract the class of pixels which represents plants' canopy automatically, considering that in some cases, the soil is colder than the plants' canopy and vice versa.

This constraint overcame using the OTSU method in TIR images and then comparing of the corresponding two classes of pixels of the RGB image used for the canopy's pixels class finding. The OTSU method was chosen because it aligns seamlessly with the challenges of thermal vineyard imagery. The natural thermal contrast between canopy leaves and soil creates a distinct difference in pixel values, resulting in a bimodal distribution that aligns with the assumptions of the OTSU method.

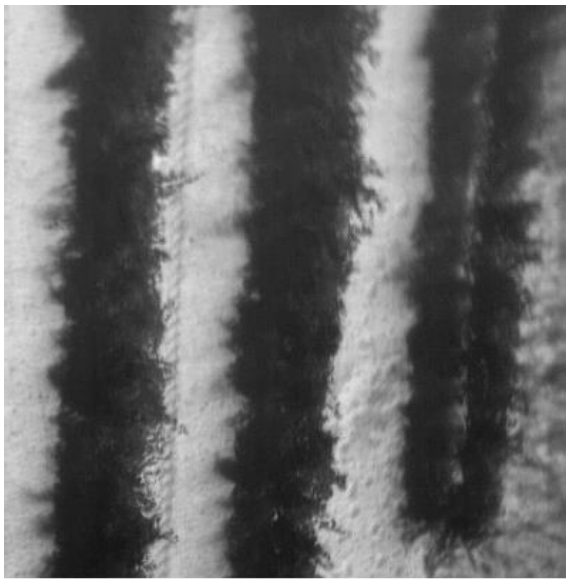

FIGURE 1. Grayscale TIR image.

Moreover, the automatic nature of the OTSU method is crucial in our approach since manual parameter setting for methods like Fuzzy C-means (FCM) is often challenging due to dynamic and variable temperature ranges. OTSU's automated threshold determination method uses data distribution to simplify parameter tuning. The method's computational efficiency and simplicity make it highly relevant to our study, especially in vineyard analysis, where soil isolation is the primary objective and resource constraints may apply.

The OTSU method's robustness makes it suitable for scenarios with well-defined pixel clusters and minimal overlap. On the other hand, FCM's consideration of membership degrees across multiple clusters may need revision when dealing with overlapping clusters. Ultimately, we opted for the OTSU method due to its compatibility with our data's unique attributes, adaptability to varying temperature profiles, computational efficiency, and resilience to scenarios with distinctive pixel clusters.

The proposed soil isolation method initially converted the TIR image to grayscale Fig. 1. Then, the OTSU method was applied to the grayscale TIR image. The OTSU algorithm assumes that the image contains two classes of pixels that follow the bimodal histogram (foreground pixels and background pixels). Then calculates the optimal threshold separating the two classes so that their combined spread (minimum variability) is minimal or equivalent (because the sum of the pairs of square distances is constant) so that their

variability is maximal [57]. This method aligns with our goal of accurately isolating soil by utilizing TIR images and the capabilities of the OTSU method.

After applying the OTSU method to the TIR images, there are two classes of pixels. However, to establish an automatic methodology for the finding of the class of pixels representing the plants' canopy was found by comparing the two classes computed by the OTSU algorithm with the corresponding classes of pixels of the cropped and aligned RGB image, which converted to Hue-Saturation-Value (HSV) color model for more precise color control than the RGB model.

E. PLANT'S CANOPY PIXELS SELECTION

The class of pixels representing the plant canopy in the TIR image was determined by selecting the corresponding class of pixels in the HSV image with the most shades of green. The class of TIR pixels representing the plant canopy is converted into a 2-D array with the temperature and coordinates of every class pixel representing the plants' canopy.

F. DATA CLUSTERING

The k-Means clustering method is used to the values of the 2-D array to group the temperatures into a specific number of groups. The k-Means method aims to optimize the manipulation of the temperatures according to the clusters where they belong, for example, a cluster of temperatures representing threshold and soil signals pixels. The most crucial part of data clustering is determining the optimum number of clusters.

1) OPTIMAL NUMBER OF CLUSTERS (k)

The elbow and Silhouette methods were used to find the most efficient number of groups (k) of the leaves' temperatures, which were retrieved from the pixels of the TIR images.

The corresponding leaves' TIR data used in the Elbow and Silhouette method was extracted from all the images of each field and flight because the absolute temperatures of the leaves differ from flight to flight. Still, there are differences between the temperatures of healthy and stressed leaves.

Furthermore, the optimum number of clusters (k) resulting from Elbow (Fig. 2) and Silhouette (Fig. 3) was the same between the different TIR data of each flight, as was expected considering the temperature differences between stressed or healthy plants.

2) ELBOW METHOD

To determine the optimal number (k) of clusters, the Elbow method uses the loss function (4) of the k-Means method. As varying the number (k) of clusters, the value of the loss function changes, and the optimal number of the clusters (k) is when the decrease of the loss function changes rapidly.

$$L = \sum_{j=1}^{k} \sum_{i=1}^{n} \left\| x_i^{(j)} - c_j \right\|^2 \tag{4}$$

3) SILHOUETTE METHOD

The silhouette method was used to find the specific number of groups during the research coefficient. Silhouette refers to

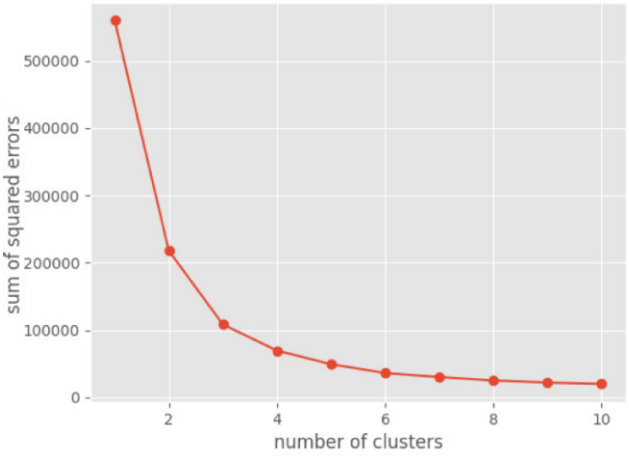

FIGURE 2. Elbow method analysis for k-Means clustering.

interpreting and validating consistency within datasets, and the technique provides a brief graphic representation of how well each item is sorted. The s(i) silhouette value (5) ranges between [1, −1], where the highest value indicates how much an object is similar to its cluster compared to neighboring clusters. The a(i) measures the similarity of point i to its cluster according to the average distance of i from all other points in the cluster. The b(i) measures the dissimilarity of point i from the points of the other clusters according to the average distance of i from the points of the closest cluster to its cluster.

$$s(i) = \frac{b(i) - a(i)}{\max\{a(i), b(i)\}} \tag{5}$$

The number of clusters (k) chosen for the method, considering the Elbow and Silhouette method, was the number six (k=6). Therefore, the values of temperatures clustered into six groups.

G. CLUSTERS VISUALIZATION

Depending on the temperature value of the cluster, each pixel's temperature value is assigned a specific color at the corresponding pixel. The colors dark green, green, light green, yellow, orange, and red are chosen and assigned hierarchically from the lowest to the highest value of each cluster and assigned in each pixel, considering the corresponding temperature value to which its cluster belongs. The purpose of standard pseudo-coloring in temperature values depending on the cluster which belongs is the standardization of every plant canopy thermal infrared footprint. Fig. 4 represents the thermal infrared footprint of a vineyard after clustering thermal values.

H. FUSION OF CLUSTERS AND RGB IMAGE

The clusters which are above the mean average temperature and represent the most significant areas of stress in the vineyards are the fourth and fifth clusters. The sixth cluster has the highest temperature values, representing the threshold pixels,

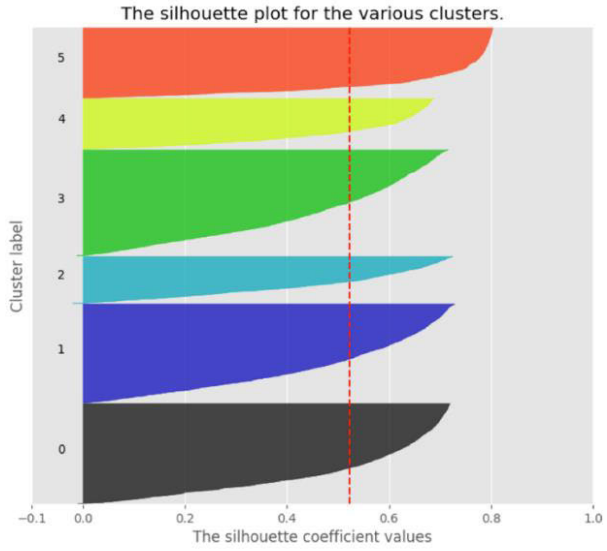

(a)

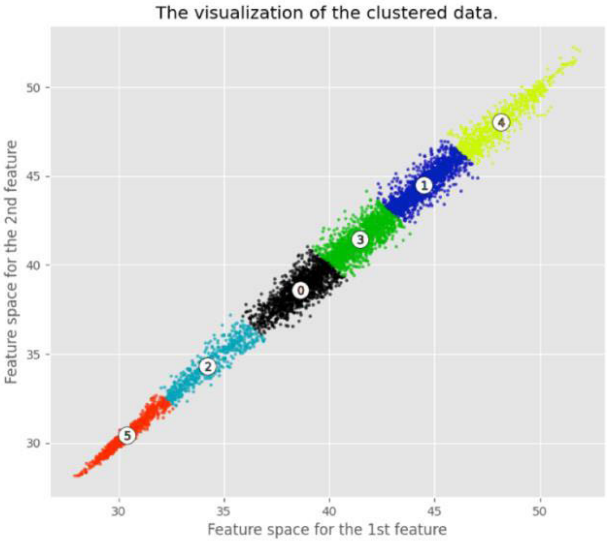

(b)

FIGURE 3. Silhouette analysis for k-Means clustering, (a) silhouette plot for the various clusters, and (b) visualization of the clustered data.

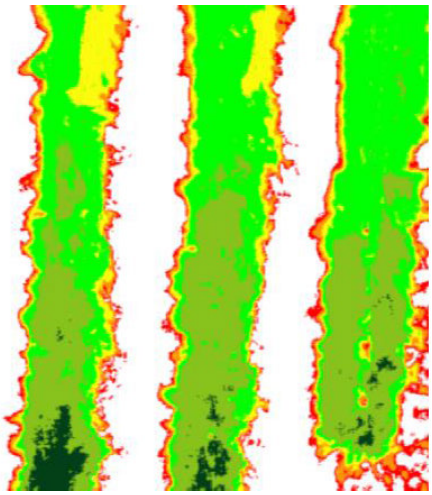

FIGURE 4. K-Means clustering of the TIR footprint.

FIGURE 5. Stressed plants pseudo-coloring visual (RGB) image.

and pixels, which are signals of soil between leaves and some weeds close to the soil, so the sixth cluster's temperature values do not depict any pixel of the vineyards' canopy leaves.

The fourth and fifth clusters' pixel coordinates are used, and a pseudo-coloring of yellow is assigned in the corresponding pixels of the aligned RGB image. Finally, an RGB image is generated with yellow pseudo-coloring over the stressed areas of the vineyards' canopy, shown in Fig. 5.

I. TGI METHOD

The TGI method was applied to all RGB images used in our proposed method for comparison. The TGI result of the vineyards' image, which is used as an example in the above methodology, is shown in Fig. 6.

Our proposed method is intended for something other than real-time application due to certain limitations and considerations regarding completion time. These constraints primarily stem from data acquisition, image processing, and analysis. The image processing steps are quite complex, particularly regarding canopy isolation and clustering, and require precise alignment between TIR and RGB images, which naturally extends the processing time. Furthermore, an end-to-end approach involving seamless image capture, data processing, and decision-making integration would streamline the solution and reduce time lag. However, implementing an end-to-end system requires further sensor technology development and computing capabilities advancements, which will involve developing real-time image analysis and decision-making

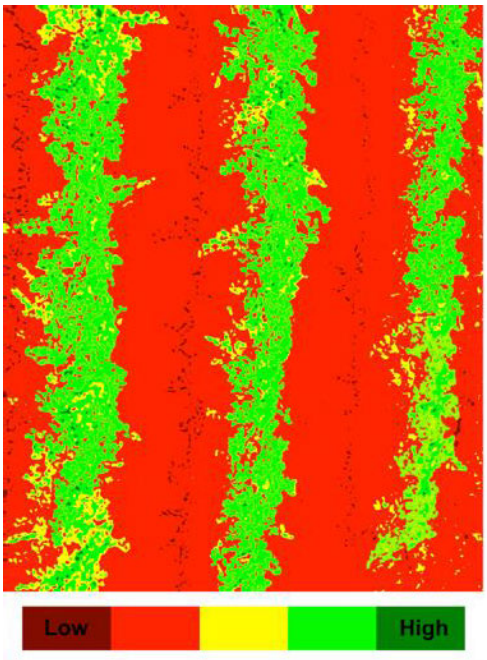

FIGURE 6. TGI pseudo-coloring of RGB image.

algorithms that operate efficiently on UAVs or edge devices. It is also essential to deploy 5G or low-latency communication infrastructure to transmit data and receive instructions in near real-time.

V. RESULTS

Our method found stressed areas in plants caused by abiotic factors, such as water stress, and biotic stress factors, such as pathogens. The dataset of the 4660 captured images was analyzed using the proposed method as well as the TGI methodology as a comparison index to reveal whether the stressed areas found by our method could be found by TGI.

The total percentage of stress area compared to the plants' canopy coverage was computed, as shown in Table 1, in the results of each flight survey. The stress percentage is computed based on the total pixels of the plant's canopy compared to the pseudo-coloring pixels, which indicate the stress area of the plant.

The proposed method found 1886 plants' stressed areas, where the TGI found 315 of them with low chlorophyll, which confirms that the first symptom in a stressed plant is stomatal closure, which proves that it needs time, depending on the abiotic or biotic factor, for the chlorophyll content decrement or the visible expression of the symptomatology.

Abiotic factors, such as water stress, constitute the reason for the most plant-stressed areas. All the stressed areas were annotated in the field after each flight for the agronomist to classify the kind of stress, abiotic or biotic, according to the plant's symptomatology expression.

One abiotic stress that is very common and the TGI was unable to identify was toxicity (Fig. 7), which is caused due

TABLE 1. Stress and plants' canopy coverage.

Date	Stress %		Plants' Canopy Coverage %	
	Mouhtaro	Merlot	Mouhtaro	Merlot
Jun-21	2.73%	2.57%	37.60%	39.28%
Jul-21	1.94%	1.89%	39.55%	40.57%
Aug-21	2.19%	1.22%	41.56%	42.71%
Jun-22	4.24%	3.87%	36.69%	38.32%
Jul-22	0.01%	0.02%	38.51%	40.49%
Aug-22	1.94%	2.24%	39.85%	41.22%

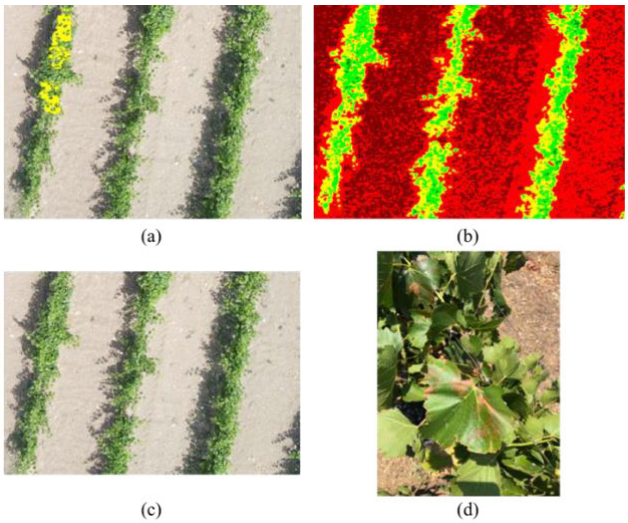

FIGURE 7. Images of a stressed plant caused by Toxicity (a) Stressed plant pseudo-coloring, (b) TGI, (c) RGB, and (d) Leaf level image.

to sulfur spraying at temperatures of approximately 30 ^{o}C degrees.

The most interesting part of the results is that the proposed method found stressed plants from 2021 without any symptom expression, and the same plants in 2022 continued to be stressed without any symptoms. In 2022 before harvest, the same plants expressed the symptoms of trunk diseases (Fig. 8). This is attributed to the fact that the trunk diseases affect the transparency of the leaves' stomata, but may express the symptoms 2-3 years after the affected day [58]. Another stressed plant with Phomopsis was found in the nascent symptomatology (Fig. 9). TGI could not identify the plants' stressed by pathogens, because the chlorophyll content decreased slightly before the symptoms' expression.

Through visual inspection, an agronomist verified the proposed method and the TGI's outcomes and categorized the stress factor type. The accuracy, precision, recall, and F1-score of both methods for each year and their overall performance are presented in Table 2. Additionally, Fig. 10 compares the evaluation metrics between the proposed

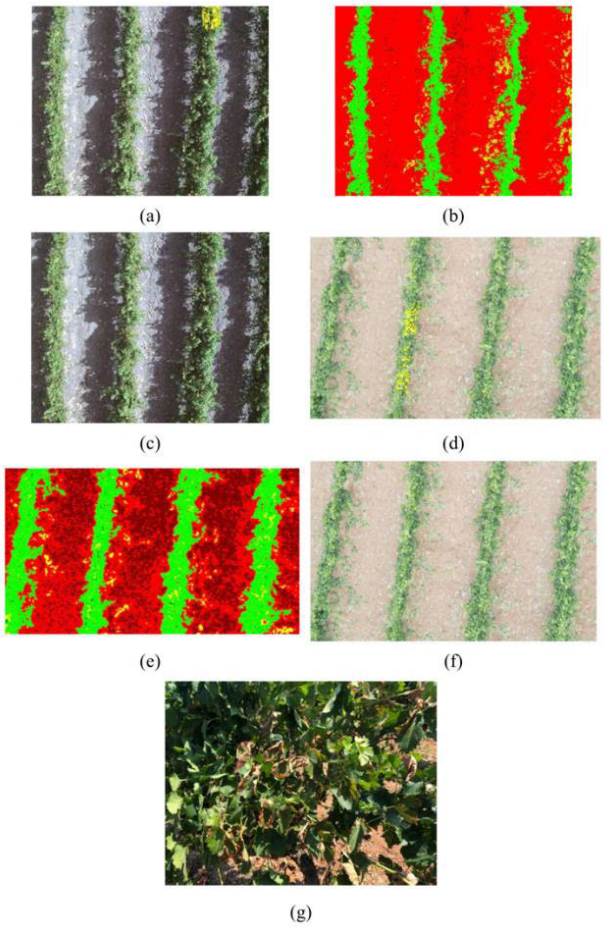

FIGURE 8. Images of the same stressed plant caused by Esca in 2021 (a) Stressed plant pseudo-coloring, (b) TGI, (c) RGB, in 2022 (d) Stressed plant pseudo-coloring, (e) TGI, (f) RGB, and (g) Leaf level image.

TABLE 2. Stress and plants' canopy coverage.

Metric	2021		2022		Cumulative of 2021-2022	
	Proposed Method	TGI	Proposed Method	TGI	Proposed Method	TGI
Accuracy	99,71%	98,95%	99,82%	90,80%	99,76%	94,88%
Precision	87,36%	90,65%	98,88%	96,15%	97,26%	94,29%
Recall	95,00%	39,27%	99,37%	12,50%	98,80%	16,08%
F1-score	91,02%	54,80%	99,12%	22,12%	98,03%	27,47%

method and TGI for each year and their cumulative performance.

In conclusion, based on the metrics outcomes, the primary variation between the proposed approach and TGI is most prominent in the recall metric for the years 2021 and 2022, and the cumulative results for both years, which were recorded as 55.73%, 86.87%, and 87.22%, respectively. Furthermore, as a consequence of the recall, the F1-score of the proposed method is better in 2021 by 36.22%, in 2022 by 77%, and in the cumulative of the two years by 70.55%.

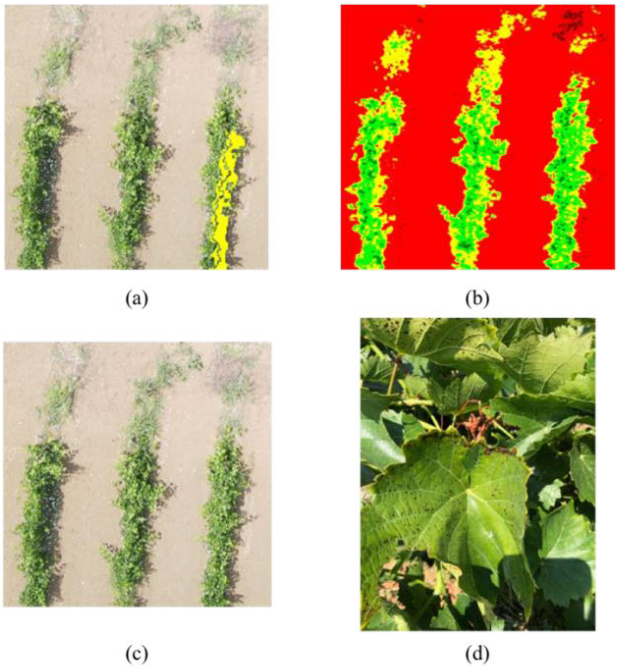

FIGURE 9. Images of a stressed plant caused by Phomopsis (a) Stressed plant pseudo-coloring, (b) TGI, (c) RGB, and (d) Leaf level image.

TABLE 3. Data specific parameters.

Specific Parameters	FLIR Duo Pro R 640		DJI Mavic 2 Enterprise Advanced	
	TIR	RGB	TIR	RGB
Focal Length	13.0mm (35 mm equivalent: 6.8 mm)	13.0mm	Approx. 9mm (35 mm equivalent: 38mm)	4.5mm (35 mm equivalent: 24.0 mm)
Resolution	640x512	4000x3000	640x512	8000x6000
Bit Depth	24	24	24	24
Megapixels	0.328	12.0	0.328	48.0
Field of View	45.0 deg	56.0 deg	24.0 deg	73.7 deg
Compression	JPEG	JPEG	JPEG	JPEG

Moreover, as per the literature review and the findings of this study, stomatal closure is the first symptom of stress in plants that are caused by biotic or abiotic factors. The proposed method can effectively identify infections in the initial stages of some pathogens, which typically take months or even years to express their symptomatology.

VI. DISCUSSION

It is known from the literature that the early symptom of a stressed plant is stomatal closure. Plants under stress may have different temperatures than healthy plants due to changes in their metabolic rate or leaf transpiration. Our method makes detecting plant stress in the early stages possible by measuring these temperature differences. Our proposed method can be used to determine and annotate

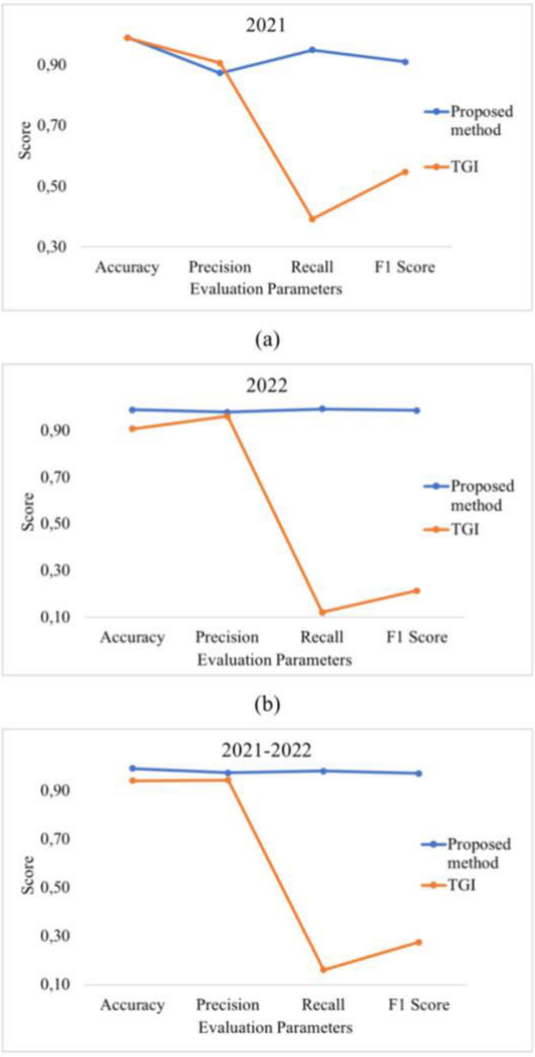

FIGURE 10. Evaluation metrics of the proposed method and TGI (a) 2021, (b) 2022, and (c) 2021-2022.

stressed areas in plants, considering that the k-means clustering is based on the relative temperatures of the leaves.

The most important conclusion of the drawn results is the early detection of the plant stress and, at most times, before the symptoms expression and with higher accuracy compared to other indexes such as TGI, which measures the chlorophyll content of the leaves. According to the results of the experimental vineyards, the proposed method found a mean of 2.07% stressed plants compared to 0.35% of plants with low chlorophyll found by the TGI method. Like all other methods and vegetation indexes, an essential constraint of the proposed method is the inability to classify the kind of stress, such as abiotic or biotic.

On the other hand, the multispectral IoT sensors measure the reflected light from the plant in multiple wavelengths, which can provide information about the plant's chlorophyll content, water content, and other factors. The indexes based on multispectral bands can detect changes in the plant's physiology that may indicate stress. However, they are often not sensitive enough to detect stress in its early stages.

Further comprehensive comparative assessments to other agricultural settings, including vertical farming and greenhouses in the future, will be conducted. The proposed method will be compared in these controlled environments with IoT matrices and different camera types, such as multispectral and hyperspectral cameras. This future work will allow the performance of our proposed method to be assessed in a broader spectrum of agricultural scenarios and facilitate meaningful comparisons with alternative techniques. Enhancing the robustness of the proposed approach through rigorous testing and validation in diverse agricultural contexts will ensure its practical applicability and effectiveness.

Future research should consider combining methods and sensors to monitor plant stress, including thermal infrared and multispectral imaging, as well as other techniques, such as monitoring the plant's growth and observing visual signs of stress, to classify the type of plant stress.

VII. CONCLUSION

We proposed a method for the early detection of plant stress according to the leaves' stomata transpiration based on TIR and RGB images which can be acquired from IoT sensors. The TIR image is the detection baseline for the stomata closure according to the relative temperatures of the plant's canopy and elimination based on the OTSU method of the soil. The RGB image was used to discriminate the plant's canopy and visualize the plant's stressed areas by pseudo-coloring. The thermal data of the TIR image are clustered according to the k-Means method, where the clusters of the plant's canopy pixels are used, excluding the soil signal or other noise.

The results of the proposed method indicate that it is highly effective to detect stressed plants before the symptoms' expression, especially when compared to methods such as TGI, which measures the leaf chlorophyll content. According to the results, abiotic factors were the most common causes of plant stress, such as water stress and toxicity caused by sulfur spraying.

In addition, biotic factors that cause plant stress were found, such as pathogens like trunk diseases that are not visible by the naked eye or other methods that measure chlorophyll content in the early stages of infection. Our method detected the plant stress caused by trunk diseases in the nascent of the infection, especially two years before symptoms expression. In this stage, the proposed method cannot classify the factors that cause plant stress, such as abiotic or biotic.

Future research should focus on combining the proposed method with other methods, such as multispectral imaging or other IoT sensors, to classify the type of stress at the time of detection. The capability of the proposed method on the early detection of stressed plants is vital to prevent further damage and improve crop yields.

ACKNOWLEDGMENT

The authors would like to thank Muses Estate for providing the vineyards for the experiments. They also like to thank all the staff for their assistance in the experimental set up. The publication of the article in OA mode was financially supported by HEAL-Link.

CONFLICT OF INTEREST

The proposed method is a part of the patent GR1009898 which Georgios Fevgas is the inventor and holder.

REFERENCES

[1] M. M. Rahaman, D. Chen, Z. Gillani, C. Klukas, and M. Chen, "Advanced phenotyping and phenotype data analysis for the study of plant growth and development," *Frontiers Plant Sci.*, vol. 6, p. 619, Aug. 2015, doi: 10.3389/fpls.2015.00619.

[2] C. Zhang and J. M. Kovacs, "The application of small unmanned aerial systems for precision agriculture: A review," *Precis. Agricult.*, vol. 13, no. 6, pp. 693–712, Dec. 2012, doi: 10.1007/s11119-012-9274-5.

[3] S. Savary, A. Ficke, J.-N. Aubertot, and C. Hollier, "Crop losses due to diseases and their implications for global food production losses and food security," *Food Secur.*, vol. 4, no. 4, pp. 519–537, Dec. 2012, doi: 10.1007/s12571-012-0200-5.

[4] R. Ballesteros, J. F. Ortega, D. Hernández, and M. A. Moreno, "Applications of georeferenced high-resolution images obtained with unmanned aerial vehicles. Part I: Description of image acquisition and processing," *Precis. Agricult.*, vol. 15, no. 6, pp. 579–592, Dec. 2014, doi: 10.1007/s11119-014-9355-8.

[5] J. Bendig, A. Bolten, S. Bennertz, J. Broscheit, S. Eichfuss, and G. Bareth, "Estimating biomass of barley using crop surface models (CSMs) derived from UAV-based RGB imaging," *Remote Sens.*, vol. 6, no. 11, pp. 10395–10412, Oct. 2014, doi: 10.3390/rs61110395.

[6] H. Al Hiary, S. B. Ahmad, M. Reyalat, M. Braik, and Z. Al Rahamneh, "Fast and accurate detection and classification of plant diseases," *Int. J. Comput. Appl.*, vol. 17, no. 1, pp. 31–38, Mar. 2011, doi: 10.5120/2183-2754.

[7] V. Singh and A. K. Misra, "Detection of plant leaf diseases using image segmentation and soft computing techniques," *Inf. Process. Agricult.*, vol. 4, no. 1, pp. 41–49, Mar. 2017, doi: 10.1016/j.inpa.2016.10.005.

[8] E. R. Hunt, P. C. Doraiswamy, J. E. Mcmurtrey, C. S. T. Daughtry, E. M. Perry, and B. Akhmedov, "A visible band index for remote sensing leaf chlorophyll content at the canopy scale," *Int. J. Appl. Earth Observ. Geoinf.*, vol. 21, pp. 103–112, Apr. 2013, doi: 10.1016/j.jag.2012.07.020.

[9] S. Candiago, F. Remondino, M. De Giglio, M. Dubbini, and M. Gattelli, "Evaluating multispectral images and vegetation indices for precision farming applications from UAV images," *Remote Sens.*, vol. 7, no. 4, pp. 4026–4047, Apr. 2015, doi: 10.3390/rs70404026.

[10] I. Colomina and P. Molina, "Unmanned aerial systems for photogrammetry and remote sensing: A review," *ISPRS J. Photogramm. Remote Sens.*, vol. 92, pp. 79–97, Jun. 2014, doi: 10.1016/j.isprsjprs.2014.02.013.

[11] R. Näsi, E. Honkavaara, P. Lyytikäinen-Saarenmaa, M. Blomqvist, P. Litkey, T. Hakala, N. Viljanen, T. Kantola, T. Tanhuanpää, and M. Holopainen, "Using UAV-based photogrammetry and hyperspectral imaging for mapping bark beetle damage at tree-level," *Remote Sens.*, vol. 7, no. 11, pp. 15467–15493, Nov. 2015, doi: 10.3390/rs71115467.

[12] K. R. Thorp, M. A. Gore, P. Andrade-Sanchez, A. E. Carmo-Silva, S. M. Welch, J. W. White, and A. N. French, "Proximal hyperspectral sensing and data analysis approaches for field-based plant phenomics," *Comput. Electron. Agricult.*, vol. 118, pp. 225–236, Oct. 2015, doi: 10.1016/j.compag.2015.09.005.

[13] P. J. Zarco-Tejada, A. Morales, L. Testi, and F. J. Villalobos, "Spatio-temporal patterns of chlorophyll fluorescence and physiological and structural indices acquired from hyperspectral imagery as compared with carbon fluxes measured with eddy covariance," *Remote Sens. Environ.*, vol. 133, pp. 102–115, Jun. 2013, doi: 10.1016/j.rse.2013.02.003.

[14] T. Ota, M. Ogawa, K. Shimizu, T. Kajisa, N. Mizoue, S. Yoshida, G. Takao, Y. Hirata, N. Furuya, T. Sano, H. Sokh, V. Ma, E. Ito, J. Toriyama, Y. Monda, H. Saito, Y. Kiyono, S. Chann, and N. Ket, "Aboveground biomass estimation using structure from motion approach with aerial photographs in a seasonal tropical forest," *Forests*, vol. 6, no. 12, pp. 3882–3898, Oct. 2015, doi: 10.3390/f6113882.

[15] L. Wallace, A. Lucieer, C. Watson, and D. Turner, "Development of a UAV-LiDAR system with application to forest inventory," *Remote Sens.*, vol. 4, no. 6, pp. 1519–1543, May 2012, doi: 10.3390/rs4061519.

[16] J. Baluja, M. P. Diago, P. Balda, R. Zorer, F. Meggio, F. Morales, and J. Tardaguila, "Assessment of vineyard water status variability by thermal and multispectral imagery using an unmanned aerial vehicle (UAV)," *Irrigation Sci.*, vol. 30, no. 6, pp. 511–522, Nov. 2012, doi: 10.1007/s00271-012-0382-9.

[17] D. Deery, J. Jimenez-Berni, H. Jones, X. Sirault, and R. Furbank, "Proximal remote sensing buggies and potential applications for field-based phenotyping," *Agronomy*, vol. 4, no. 3, pp. 349–379, Jul. 2014, doi: 10.3390/agronomy4030349.

[18] V. Gonzalez-Dugo, P. Hernandez, I. Solis, and P. Zarco-Tejada, "Using high-resolution hyperspectral and thermal airborne imagery to assess physiological condition in the context of wheat phenotyping," *Remote Sens.*, vol. 7, no. 10, pp. 13586–13605, Oct. 2015, doi: 10.3390/rs71013586.

[19] H. G. Jones, R. Serraj, B. R. Loveys, L. Xiong, A. Wheaton, and A. H. Price, "Thermal infrared imaging of crop canopies for the remote diagnosis and quantification of plant responses to water stress in the field," *Funct. Plant Biol.*, vol. 36, no. 11, p. 978, 2009, doi: 10.1071/FP09123.

[20] R. Sugiura, N. Noguchi, and K. Ishii, "Correction of low-altitude thermal images applied to estimating soil water status," *Biosyst. Eng.*, vol. 96, no. 3, pp. 301–313, Mar. 2007, doi: 10.1016/j.biosystemseng.2006.11.006.

[21] R. D. Jackson, "Remote sensing of biotic and abiotic plant stress," *Annu. Rev. Phytopathol.*, vol. 24, no. 1, pp. 265–287, Sep. 1986, doi: 10.1146/annurev.py.24.090186.001405.

[22] S. Khanal, J. Fulton, and S. Shearer, "An overview of current and potential applications of thermal remote sensing in precision agriculture," *Comput. Electron. Agricult.*, vol. 139, pp. 22–32, Jun. 2017, doi: 10.1016/j.compag.2017.05.001.

[23] A.-K. Mahlein, "Plant disease detection by imaging sensors—Parallels and specific demands for precision agriculture and plant phenotyping," *Plant Disease*, vol. 100, no. 2, pp. 241–251, Feb. 2016, doi: 10.1094/PDIS-03-15-0340-FE.

[24] H. G. Jones and R. A. Vaughan, *Remote Sensing of Vegetation: Principles, Techniques, and Applications*. USA: OUP Oxford, 2010.

[25] M. Gerhards, M. Schlerf, K. Mallick, and T. Udelhoven, "Challenges and future perspectives of multi-/hyperspectral thermal infrared remote sensing for crop water-stress detection: A review," *Remote Sens.*, vol. 11, no. 10, p. 1240, May 2019, doi: 10.3390/rs11101240.

[26] S. B. Idso, R. D. Jackson, P. J. Pinter, R. J. Reginato, and J. L. Hatfield, "Normalizing the stress-degree-day parameter for environmental variability," *Agric. Meteorol.*, vol. 24, pp. 45–55, Jan. 1981, doi: 10.1016/0002-1571(81)90032-7.

[27] P. J. Zarco-Tejada, C. Camino, P. S. A. Beck, R. Calderon, A. Hornero, R. Hernández-Clemente, T. Kattenborn, M. Montes-Borrego, L. Susca, M. Morelli, V. Gonzalez-Dugo, P. R. J. North, B. B. Landa, D. Boscia, M. Saponari, and J. A. Navas-Cortes, "Previsual symptoms of *Xylella fastidiosa* infection revealed in spectral plant-trait alterations," *Nature Plants*, vol. 4, no. 7, pp. 432–439, Jun. 2018, doi: 10.1038/s41477-018-0189-7.

[28] P. J. Zarco-Tejada, V. González-Dugo, and J. A. J. Berni, "Fluorescence, temperature and narrow-band indices acquired from a UAV platform for water stress detection using a micro-hyperspectral imager and a thermal camera," *Remote Sens. Environ.*, vol. 117, pp. 322–337, Feb. 2012, doi: 10.1016/j.rse.2011.10.007.

[29] M. P. Fuller and M. Wisniewski, "The use of infrared thermal imaging in the study of ice nucleation and freezing of plants," *J. Therm. Biol.*, vol. 23, no. 2, pp. 81–89, Apr. 1998, doi: 10.1016/S0306-4565(98)00013-8.

[30] M. Stegner, T. Schäfernolte, and G. Neuner, "New insights in potato leaf freezing by infrared thermography," *Appl. Sci.*, vol. 9, no. 5, p. 819, Feb. 2019, doi: 10.3390/app9050819.

[31] J. M. Costa, R. Egipto, A. Sánchez-Virosta, C. M. Lopes, and M. M. Chaves, "Canopy and soil thermal patterns to support water and heat stress management in vineyards," *Agricult. Water Manage.*, vol. 216, pp. 484–496, May 2019, doi: 10.1016/j.agwat.2018.06.001.

[32] R. Pan, W. Jiang, Q. Wang, L. Xu, S. Shabala, and W. Y. Zhang, "Differential response of growth and photosynthesis in diverse cotton genotypes under hypoxia stress," *Photosynthetica*, vol. 57, no. 3, pp. 772–779, Jul. 2019, doi: 10.32615/ps.2019.087.

[33] L. Chaerle, D. Hagenbeek, X. Vanrobaeys, and D. Van Der Straeten, "Early detection of nutrient and biotic stress in phaseolus vulgaris," *Int. J. Remote Sens.*, vol. 28, no. 16, pp. 3479–3492, Aug. 2007, doi: 10.1080/01431160601024259.

[34] V. I. Myers, L. R. Ussery, and a. W. J. Rippert, "Photogrammetry for detailed detection of drainage and salinity problems," *Trans. ASAE*, vol. 6, no. 4, pp. 0332–0334, 1963, doi: 10.13031/2013.40907.

[35] Z. S. Siddiqui, J.-I. Cho, S.-H. Park, T.-R. Kwon, G.-S. Lee, M.-J. Jeong, K.-W. Kim, S.-K. Lee, and S.-C. Park, "Phenotyping of rice in salt stress environment using high-throughput infrared imaging," *Acta Botanica Croatica*, vol. 73, no. 1, pp. 312–321, Apr. 2014, doi: 10.2478/botcro-2013-0027.

[36] X. R. R. Sirault, R. A. James, R. T. Furbank, X. R. R. Sirault, R. A. James, and R. T. Furbank, "A new screening method for osmotic component of salinity tolerance in cereals using infrared thermography," *Funct. Plant Biol.*, vol. 36, no. 11, pp. 970–977, Nov. 2009, doi: 10.1071/FP09182.

[37] P. J. Pinter, M. E. Stanghellini, R. J. Reginato, S. B. Idso, A. D. Jenkins, and R. D. Jackson, "Remote detection of biological stresses in plants with infrared thermometry," *Science*, vol. 205, no. 4406, pp. 585–587, Aug. 1979, doi: 10.1126/science.205.4406.585.

[38] H. E. Sveriges and L. Nilsson. (1985). *Remote Sensing of Oil Seed Rape Infected by Sclerotinia Stem Rot and Verticillium Wilt. [Sclerotina Sclerotiorum, Verticillium Dahliae, Spectral Signatures]*. Vaextskyddsrapporter Jordbr. Swed. Accessed: Dec. 10, 2020. [Online]. Available: https://agris.fao.org/agris-search/search.do?recordID=SE8640006

[39] L. Wang, S. Poque, and J. P. T. Valkonen, "Phenotyping viral infection in sweetpotato using a high-throughput chlorophyll fluorescence and thermal imaging platform," *Plant Methods*, vol. 15, no. 1, p. 116, Oct. 2019, doi: 10.1186/s13007-019-0501-1.

[40] S. Joalland, C. Screpanti, F. Liebisch, H. V. Varella, A. Gaume, and A. Walter, "Comparison of visible imaging, thermography and spectrometry methods to evaluate the effect of *Heterodera schachtii* inoculation on sugar beets," *Plant Methods*, vol. 13, no. 1, p. 73, Sep. 2017, doi: 10.1186/s13007-017-0223-1.

[41] C. M. Ortiz-Bustos, M. L. Perez-Bueno, M. Barón, and L. Molinero-Ruiz, "Use of blue-green fluorescence and thermal imaging in the early detection of sunflower infection by the root parasitic weed *Orobanche cumana* Wallr," *Frontiers Plant Sci.*, vol. 8, p. 833, May 2017. [Online]. Available: https://www.frontiersin.org/articles/10.3389/fpls.2017.00833

[42] V. Gonzalez-Dugo, P. Zarco-Tejada, E. Nicolás, P. A. Nortes, J. J. Alarcón, D. S. Intrigliolo, and E. Fereres, "Using high resolution UAV thermal imagery to assess the variability in the water status of five fruit tree species within a commercial orchard," *Precis. Agricult.*, vol. 14, no. 6, pp. 660–678, Dec. 2013, doi: 10.1007/s11119-013-9322-9.

[43] J. A. J. Berni, P. J. Zarco-Tejada, G. Sepulcre-Cantó, E. Fereres, and F. Villalobos, "Mapping canopy conductance and CWSI in olive orchards using high resolution thermal remote sensing imagery," *Remote Sens. Environ.*, vol. 113, no. 11, pp. 2380–2388, Nov. 2009, doi: 10.1016/j.rse.2009.06.018.

[44] J. A. J. Berni, P. J. Zarco-Tejada, L. Suarez, and E. Fereres, "Thermal and narrowband multispectral remote sensing for vegetation monitoring from an unmanned aerial vehicle," *IEEE Trans. Geosci. Remote Sens.*, vol. 47, no. 3, pp. 722–738, Mar. 2009, doi: 10.1109/TGRS.2008.2010457.

[45] N. R. Falkenberg, G. Piccinni, J. T. Cothren, D. I. Leskovar, and C. M. Rush, "Remote sensing of biotic and abiotic stress for irrigation management of cotton," *Agricult. Water Manag.*, vol. 87, no. 1, pp. 23–31, Jan. 2007, doi: 10.1016/j.agwat.2006.05.021.

[46] B. Cohen, Y. Edan, A. Levi, and V. Alchanatis, "Early detection of grapevine *(Vitis vinifera)* downy mildew (Peronospora) and diurnal variations using thermal imaging," *Sensors*, vol. 22, no. 9, p. 3585, May 2022, doi: 10.3390/s22093585.

[47] M. Smigaj, R. Gaulton, J. C. Suárez, and S. L. Barr, "Canopy temperature from an unmanned aerial vehicle as an indicator of tree stress associated with red band needle blight severity," *Forest Ecology Manag.*, vol. 433, pp. 699–708, Feb. 2019, doi: 10.1016/j.foreco.2018.11.032.

[48] Y. Wang, S. Zia-Khan, S. Owusu-Adu, T. Miedaner, and J. Müller, "Early detection of zymoseptoria tritici in winter wheat by infrared thermography," *Agriculture*, vol. 9, no. 7, p. 139, Jul. 2019, doi: 10.3390/agriculture9070139.

[49] J. Park and K. W. Kim, "Outdoor infrared imaging for spatial and temporal thermography: A case study of necrotic versus healthy leaf areas on woody plants," *J. Phytopathol.*, vol. 169, no. 1, pp. 62–70, Jan. 2021, doi: 10.1111/jph.12959.

[50] M. López-López, R. Calderón, V. González-Dugo, P. Zarco-Tejada, and E. Fereres, "Early detection and quantification of almond red leaf blotch using high-resolution hyperspectral and thermal imagery," *Remote Sens.*, vol. 8, no. 4, p. 276, Mar. 2016, doi: 10.3390/rs8040276.

[51] L. Zhang, Y. Niu, H. Zhang, W. Han, G. Li, J. Tang, and X. Peng, "Maize canopy temperature extracted from UAV thermal and RGB imagery and its application in water stress monitoring," *Frontiers Plant Sci.*, vol. 10, p. 1270, Oct. 2019, doi: 10.3389/fpls.2019.01270.

[52] M. Fuchs and C. B. Tanner, "Infrared thermometry of vegetation," *Agronomy J.*, vol. 58, no. 6, pp. 597–601, Nov. 1966, doi: 10.2134/agronj1966.00021962005800060014x.

[53] J. W. Salisbury and D. M. D'Aria, "Emissivity of terrestrial materials in the 8–14 μm atmospheric window," *Remote Sens. Environ.*, vol. 42, no. 2, pp. 83–106, Nov. 1992, doi: 10.1016/0034-4257(92)90092-X.

[54] R. Giuliani and J. A. Flore, "Potential use of infra-red thermometry for the detection of water stress in apple trees," *Acta Horticulturae*, vol. 537, pp. 383–392, Oct. 2000. [Online]. Available: https://www.cabdirect.org/cabdirect/abstract/20003033244

[55] I. Leinonen and H. G. Jones, "Combining thermal and visible imagery for estimating canopy temperature and identifying plant stress," *J. Experim. Botany*, vol. 55, no. 401, pp. 1423–1431, Jun. 2004, doi: 10.1093/jxb/erh146.

[56] M. Moller, V. Alchanatis, Y. Cohen, M. Meron, J. Tsipris, A. Naor, V. Ostrovsky, M. Sprintsin, and S. Cohen, "Use of thermal and visible imagery for estimating crop water status of irrigated grapevine," *J. Experim. Botany*, vol. 58, no. 4, pp. 827–838, Nov. 2006, doi: 10.1093/jxb/erl115.

[57] N. Otsu, "A threshold selection method from gray-level histograms," *IEEE Trans. Syst., Man, Cybern.*, vol. SMC-9, no. 1, pp. 62–66, Jan. 1979, doi: 10.1109/TSMC.1979.4310076.

[58] G. Surico, G. Marchi, P. Braccini, and L. Mugnai, "Epidemiology of esca in some vineyards in Tuscany (Italy)," *Phytopathol. Mediterr.*, vol. 39, no. 1, pp. 190–205, 2000.

GEORGIOS FEVGAS received the B.S. degree in aeronautical sciences from the Hellenic Air Force Academy, Athens, Greece, in 2013. He is currently pursuing the Ph.D. degree with the Department of Computer Science, International Hellenic University. He is the inventor of a patent that combines smart farming, computer vision, and artificial intelligence. His research interests include remote sensing, the IoT, computer vision, artificial intelligence, and unmanned aerial vehicles (UAVs).

THOMAS LAGKAS (Senior Member, IEEE) received the degree (Hons.) from the Department of Informatics, Aristotle University of Thessaloniki, in 2002, the Ph.D. degree in wireless networks from the Department of Informatics, Aristotle University of Thessaloniki, in 2006, and the M.B.A. degree from Hellenic Open University, in 2012. He received a postgraduate certificate on teaching and learning from The University of Sheffield, in 2017. He was a Scholar with the Aristotle University Research Committee and a Postdoctoral Scholar with the National Scholarships Institute of Greece. He is currently an Assistant Professor with the Department of Computer Science, International Hellenic University. He is a fellow with the Higher Education Academy, U.K. His research interests include the IoT communications with more than 140 (and over 2000 citations) publications at a number of widely recognized international scientific journals and conferences. Moreover, he actively participates in the preparation, management, and implementation of several EU funded research projects.

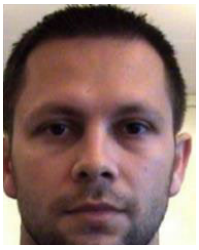

VASILEIOS ARGYRIOU (Member, IEEE) received the B.Sc. degree in computer science from the Aristotle University of Thessaloniki, Greece, in 2001, and the M.Sc. and Ph.D. degrees in electrical engineering working on registration from the University of Surrey, in 2003 and 2006, respectively. From 2001 to 2002, he held a research position with Aristotle University, with a focus on image and video watermarking. He joined the Communications and Signal Processing Department, Imperial College London, London, in 2007, where he was a Research Fellow working on 3D object reconstruction. He is currently a Professor with Kingston University, London, working on computer vision and AI for crowd and human behavior analysis, computer games, entertainment, and medical applications. Also, research is conducted on educational games and on HCI for augmented and virtual reality (AR/VR) systems.

PANAGIOTIS SARIGIANNIDIS (Member, IEEE) received the B.Sc. and Ph.D. degrees in computer science from the Aristotle University of Thessaloniki, Thessaloniki, Greece, in 2001 and 2007, respectively. He is currently the Director of the ITHACA Laboratory, the Co-Founder of the first spin-off of the University of Western Macedonia: MetaMind Innovations P.C., and an Associate Professor with the Department of Electrical and Computer Engineering, University of Western Macedonia, Kozani, Greece. He has published over 260 papers in international journals, conferences, and book chapters, including IEEE Communications Surveys and Tutorials, IEEE Transactions on Communications, IEEE Internet of Things Journal, IEEE Transactions on Broadcasting, IEEE Systems Journal, *IEEE Wireless Communications Magazine*, IEEE Open Journal of the Communications Society, IEEE/OSA Journal of Lightwave Technology, IEEE Transactions on Industrial Informatics, IEEE Access, and *Computer Networks*. He has been involved in several national, European, and international projects. He is also the Project Coordinator of three H2020 Projects; 1) H2020-DS-SC7-2017 (DS-07-2017), SPEAR: Secure and PrivatE smArt gRid; 2) H2020-LC-SC3-EE-2020-1 (LC-SC3-EC-4-2020), EVIDENT: bEhaVioral Insgihts anD Effective eNergy policy acTions; and 3) H2020-ICT-2020-1 (ICT-56-2020), TERMINET: nexT gEneRation sMart INterconnectEd ioT, while he coordinates the Operational Program MARS: sMart fArming with dRoneS (Competitiveness, Entrepreneurship, and Innovation) and the Erasmus+ KA2 ARRANGE-ICT: SmartROOT: Smart faRming innOvatiOn Training. He also serves as a Principal Investigator of the H2020-SU-DS-2018 (SU-DS04-2018), SDN-microSENSE: SDN-microgrid reSilient Electrical eNergy SystEm and in three Erasmus+ KA2: 1) ARRANGE-ICT: pArtneRship foR AddressiNG mEgatrends in ICT; 2) JAUNTY: Joint undergAduate coUrses for smart eNergy managemenT sYstems; and 3) STRONG: advanced firST RespONders trainiG (Cooperation for Innovation and the Exchange of Good Practices). His research interests include telecommunication networks, the Internet of Things, and network security. He participates in the editorial boards of various journals.